applied sciences

MDPI

*Article*

# Laboratorial Simulation for Assessing the Performance of Slates as Construction Materials in Cold Climates

**Fabio Sitzia [1,2,*], Carla Lisci [1,2], Vera Pires [1,3], Tiago Alves [2] and José Mirão [1,2]**

[1] HERCULES Laboratory, University of Évora, Largo Marquês de Marialva 8, 7000-809 Évora, Portugal
[2] Geosciences Department, School of Sciences and Technology, University of Évora, Rua Romão Ramalho 59, 7000-671 Évora, Portugal
[3] LEM Laboratório de Ensaios Mecânicos, Universidade de Évora, R. Romão Ramalho 59, 7000-671 Évora, Portugal
* Correspondence: fsitzia@uevora.pt

**Abstract:** This paper presents the results of a laboratory simulation of a subarctic climate carried out in climatic chamber. Realistic daily and seasonal cycles of temperature of a regular subarctic continental climate without dry seasons (Dfc) were simulated and the physical/mechanical properties and performance of the slates were assessed. The slate was selected because of its use as cladding and roofing material in cold regions. Mechanical performances before and after Dfc climate simulation were evaluated through point load index, uniaxial compression, flexural strength and anchor rupture load. A decrease in these mechanical features between 9 and 50% with respect to the initial strengths has been registered. Other physical parameters such as apparent density, open porosity and water absorption were evaluated. The tests showed an increase in open porosity (+72%) and a decrease in bulk density (−0.7%). The results highlighted a predominantly physical decay and mechanical performance decreasing with a relevant lowering in strength without the detection of chemical–mineralogical alterations. Moreover, artificial sun exposure reproduced the weak solar radiation that characterizes the Dfc climate. This was carried out to assess the aesthetic characteristics of the slate, since discoloration under sun exposure was supposed to occur but the slates did not exhibit substantial color changes.

**Keywords:** subarctic climate; weathering; solar radiation exposure; slate; cladding; roofing



**Citation:** Sitzia, F.; Lisci, C.; Pires, V.; Alves, T.; Mirão, J. Laboratorial Simulation for Assessing the Performance of Slates as Construction Materials in Cold Climates. *Appl. Sci.* **2023**, *13*, 2761. https://doi.org/10.3390/app13052761

Academic Editor: Muhammad Junaid Munir

Received: 3 February 2023
Revised: 17 February 2023
Accepted: 18 February 2023
Published: 21 February 2023



## 1. Introduction

Natural stones and other commonly resistant construction materials can be damaged in cold climatic conditions.

According to the Köppen classification [1], the subarctic climate (also identified as subpolar or boreal; abbreviated Dfc) is characterized by long winters and cold and short summers. This climate usually occurs on large intracontinental landmasses, often away from the mitigating effects of oceans, mainly between 50° and 70° N latitude.

Subarctic climates are represented by the Köppen climate classification, and they are divided into six categories: Dfc, Dwc, Dsc, Dfd, Dwd, and Dsd [1]. Based on Köppen's description, the first D letter indicates a continental climate where the temperature of the warmest month is $\geq$10 °C, and the temperature of the coldest month is $\leq -3$ °C. The second letter indicates: s = dry summer, w = dry winter, and f = without dry season. The third letter denotes temperature: c = regular subarctic and d = severely cold subarctic.

The Dfc climate is by far the most common subarctic type and is the one selected in this study (Figure 1). It has so far been found in the majority of Siberia, Fennoscandia, some portions of central Romania and Germany, Alaska, Labrador, Ontario, and the Canadian Prairies [2]. At middle latitudes, it can be found on the orogenic-like Alps and Pyrenees at elevations of 1600 < Z < 2100 m a.s.l. [3,4].

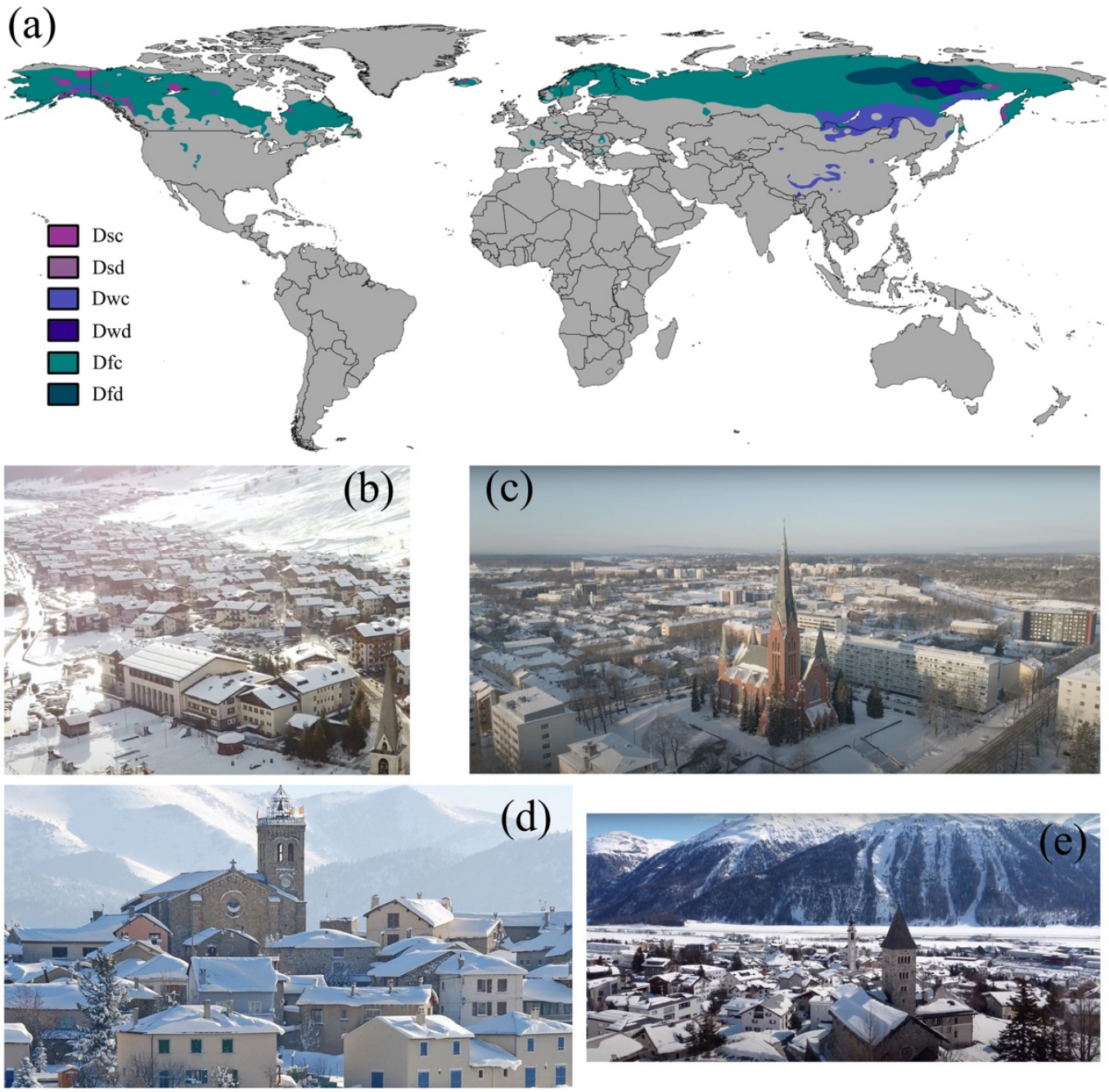


**Figure 1.** (**a**) Worldwide distribution of subarctic climate according to Köppen [1]; (**b**) Livigno (Italy); (**c**) Turku (Finland); (**d**) Les Angles (France); (**e**) Samedan (Switzerland) during winter.

Most of the subarctic climate sites show little precipitation that never exceeds 380 mm/year. Differently from hot–mild (Csa, Csb) or humid continental regions (Dfa, Dfb), in coastal areas with a subarctic climate and also in subarctic climate areas far from the coast, precipitation occurs mostly in the warmer summer months [3].

Subarctic climate regions are normally considered unwelcoming even if ancient and contemporary human settlements are present in these zones [5]. Examples of extreme temperatures in Dfc climate zones were registered in: Livigno, Italy (−37 °C); Tatra Mountains, Poland (−40 °C); Petropavlovsk-Kamchatskiy, Russia (−31.7 °C); and Old Crow, Canada (−59.4 °C). Such considerably low temperatures have a strong damaging effect on stone building materials. In this paper, the results of a laboratory simulation of a subarctic climate, carried out in a climatic chamber, are presented.

*Slate and Other Building Materials Performance at Low Temperatures*

Slate is quarried in several European countries (e.g., England, France, Italy, Spain, Belgium and Portugal) and is marketed all over the world. Together with quartzites, hornfels, and gabbros, it is one of the most durable stones in cold climate regions and used in mountain localities throughout Europe for roofing (Figure 2a), coverings, and wall ashlars, thus representing a typical example of the use of local and traditional raw materials in vernacular architecture [6,7].


**Figure 2.** (**a**,**c**) Examples of slates used for roofing applications and associated damage due to snow accumulation; (**b**) damage due to frost action photo credits by Marco Argiolas.

Slates are formed by low- or very low-grade metamorphism that gives them slaty cleavage, where phyllosilicate minerals are the predominant components of the rock. Slates are relatively light and characterized by good fissility that allows them to split into tiles and, most importantly, to have good waterproofing properties [8,9]. Some slates are particularly prone to deterioration (Figure 2b,c), especially in cases of sand intercalation, microfractures, and a high presence of carbonates. These compounds may affect the slate's physical, mechanical, and aesthetic quality in different ways: by reducing waterproofing and resistance to mechanical stress; by making slate laying difficult and making the fit between slates imperfect; and by affecting the aesthetic appearance of the slab [10].

The available standard test method to evaluate natural stone frost resistance is the EN 12371 (determination of frost resistance). According to this standard, specimens are subjected to controlled freezing and thawing conditions with temperatures ranging from −20 °C to 20 °C and from 14 to 168 cycles according to the stone integrity. According to the EN 12371 standard, two options are available to evaluate frost resistance: (i) A technological test—in which frost resistance is assessed based on the mechanical performance changes in compression or flexural strength or anchorage rupture load, before and after the cycles.

A visual inspection can also be included. (ii) An identification test—initial and periodic (after 14, 56, 84, 140, and 168 cycles, for example) visual inspection and dynamic Young's modulus assessment. There is also the option of apparent volume measurement comparison before and after the selected number of cycles. This standard has been commonly used by some authors [10–17] who have detected a loss in weight due to decohesion and an overall reduction in mechanical properties (e.g., ultrasound wave velocity and uniaxial compressive strength).

In our research, an innovative experimental climatic chamber setup was followed based upon EN 12371 standard principles on freeze–thaw, but with added parameters that are not included in this standard such as rain and temperature of a subpolar Dfc climate, aiming to artificially reproduce the four seasons in the climatic chamber. As far as the authors are aware, this is the first time the Dfc climate has been reproduced in the laboratory with the aim of foreseeing the behavior of natural stone in buildings in extreme weathering conditions.

Moreover, this study includes the analysis of aesthetic parameters, in terms of color changes of the slate exposed to the Dfc climate solar radiation, by an aging test in a SOLARBOX climatic chamber. According to the statements of the quarrymen and traders of slate, its discoloration over time happens under solar radiation exposure. The aim of this study is to verify these statements. However, the process of natural stone discoloration when exposed to solar radiation is already known [18]. Dark-colored stones change to light shades while the latter change to dark shades following exposure [19]. Overall, natural stone color variation strictly depends on the color variation of the mineralogical phases comprising the stone, as further discussed in [20].

To realistically reproduce in the laboratory the climatic conditions of Dfc climate regions, the meteorological station data of Livigno, Italy (46°32′17.42″ N–10°08′09.57″ E, Z = 1826 m s.l.m.) were selected as an example in terms of air temperature and precipitation.

To obtain reliable experimental data on natural stone aging under simulated conditions, seasonal cycles with a total duration of one month for each of the four seasons were programmed with temperatures and drying–wetting–frost conditions.

Point load, compression/flexural strength, anchor rupture load, apparent density, and open porosity were evaluated before and after the complete sequence of winter, spring, summer, and autumn in the climate chamber.

Aging tests on natural stones with realistic climatic conditions have already been carried out mimicking the Mediterranean Csa [19,21,22], the humid continental (Dfb), and the temperate oceanic (Cfb) [23] climates. All these studies aimed to investigate the suitability of artificial climatic conditions on reproducing a particular climate in the laboratory and to analyze the level of changes achieved in natural stone materials. The authors had also carried out a study of the physical properties and mechanical performance of slate materials with the objective of understanding the influence of anisotropy on flexural and dowel–hole rupture loads [24].

In manufactured stone materials such as concrete and mortars, the action of low temperature is well known in the literature and is similar to the stones [9,25]. Concrete and mortars are heterogeneous systems consisting of an open and closed pore framework, and due to this the ice crystallization pressure during freeze–thaw cycles is one of the main degradation causes [26,27].

Ice crystallization inside the porous network is mainly regulated by open porosity, permeability and pore tortuosity [12]. In general, in porous materials, the freeze–thaw cycles are responsible for an increase in porosity mostly due to pore enlargement by the volumetric expansion of the ice. The movement of water from smaller pores or unfrozen areas to growing ice crystals in larger pores is also identified as the main cause of the formation of stresses by capillary and hydraulic pressures [28]. However, it is accepted as a basic requirement for the development of damage due to frost action in porous media, that the stresses induced by ice crystallization exceed the tensile strength of the material [28]. These stresses are aggravated when salts are dissolved in the solution and

then can crystallize inside the porous framework [29,30]. As a result, porosity increasing together with spalling and other physical decay processes reduce the resistant section of a concrete artifact such as a column or a pillar. The same mechanisms act on natural stones and mortars [31,32]. These effects successively lower the compression strength in the case of a natural stone column and the flexure strength in the case of a cladding slab [33].

As mentioned above, the freeze–thaw effects on natural stone have been studied by several authors in both laboratory simulations, strictly following the EN 12371 method, and on-site analyses. The novelty of our study is the fact that a cold climate condition for a subpolar Dfc climate was simulated in a climatic chamber reproducing the four seasons based upon available real climatic data on temperature and rain. Moreover, the aging evaluation test was performed through other evaluation methods besides the ones recommended by the European standard: roughness, point load index, and P-wave ultrasound speed. In addition, this study includes the analysis of aesthetic parameters, in terms of color changes of the slate exposed to the Dfc climate solar radiation in SOLARBOX climatic chamber. To the authors' knowledge, this is the first time the Dfc climate has been realistically reproduced in the laboratory with the aim of foreseeing the behavior of natural stones in buildings in extreme conditions. With this study, the authors aimed to fill a gap in the climatic chamber simulation aging test based upon real climatic parameters. This study could be replicated in several other climates and also increases the knowledge of potential climate change effects on natural stone performance.

## 2. Slate Materials in European Building Sector

### *2.1. Slate Employment in Building Sector: Yesterday and Today*

Since antiquity, slate has been used with the aim of manufacturing small and medium-sized artifacts up to large-scale use in ancient and contemporary buildings [34]. It is believed that it was first used about two thousand two hundred years ago around northern Italy. Although it was common in Roman times, its use is antecedent to the roman empire. In Italy, there are necropolises made up of "box" tombs entirely made with this material (VIII–VII century B.C.).

In the Fontanabuona Valley (Italy), the first slate deposits have been intensively exploited starting from the XII century and the middle of the IX century. Other quarries in Europe are located near Angers, Grenoble, Cherbourg (France), Wales in the United Kingdom, Portugal, Norway, Belgium, Germany, and Spain [35].

The massive appearance of slate in Europe replaced the use of brick roof tiles [36]. At the end of the XIV century A.D., slate with blue reflections was extracted in Italy, France, and England [37]. This slate had the characteristic of shining under the sun on sunny days. In England, where blue slate was exported, cyan was considered a pure and expensive color [38]. In France itself, blue was also the color of royalty. Inevitably, this made blue slate a semi-precious and expensive material.

Slate originating from Portugal, belonging to Valongo, is used for the most varied applications. This region saw its exploitation advance due to an industrialized extraction regime in the middle of the XIX century with the arrival of the English company VS&MQC in this area [39].

In Germany, Hunsrück slate was quarried over several centuries. Archaeological finds in the western part of Germany show that slate was used in Roman times [40]. The first documented mining dates from the XIV century, and the production continued with the Industrial Revolution at the end of the 1700s, but in 1846–1849 the industry faced a serious crisis.

In Norway, traces of the use of slate in construction have been ascertained during the Neolithic period from the north to the south of the country [41].

Although slate employment in Europe has never definitively faded, it had a slight decline during the first Industrial Revolution. Its use today is mainly in mountain regions (Figure 2). Here, slate is used as cladding and roofing material of ancient buildings belonging to historic urban centers. Its application is due to the ease of dividing the material

into thin, flat, light, and waterproof slabs that are sufficiently resistant to atmospheric agents. Its black color also has an albedo close to zero and, in areas with cold climates, allows it to absorb the sun's heat and warm up in a convenient way. Typically, the criteria used for damage assessment caused by frost are those described by the EN 12371 standard test method. A possible damage classification can be performed following the visual inspection criteria described in this document: 0—no visible damage; 1—very minor damage (small rounding of vertices and edges) that do not compromise the integrity of the specimen; 2—one or several small cracks ($\leq$0.1 mm wide) or small fragments detached ($\leq$30 mm$^2$ per fragment); 3—one or more cracks, holes, or detachment of fragments larger than those defined for classification "2", or a change in the material of the veins, or the test piece shows important signs of disintegration or dissolution; and 4—specimen with large cracks or broken into two or more pieces or disintegrated. Still, it is important to highlight that currently there is no European standard for natural stone inspection and maintenance.

### *2.2. Petrographic Characteristics of Slate*

The slate used in our research belongs to the Valongo region (Portugal), which has an age of 350 million years (Carboniferous period) [42]. The physical–mechanical behavior and the alteration modalities of Portuguese slate are common in the other slates of European origin.

Slate is a metamorphosed rock of sedimentary origin (epidote–pumpellyite facies). The metamorphism is regionally low-grade. The rock presents a porphyro-lepidoblastic texture (Figure 3a–d). By polarized microscope (OM) observations, a large fraction of black-colored organic matter was detected. The paragenesis shows phyllosilicates (e.g., muscovite and clinochlore), quartz, and opaques. Furthermore, semi-quantitative analyses by X-ray diffraction (XRD) patterns (Figure 3e) highlighted the peaks corresponding to the mineralogical composition: muscovite (22.3%), clinochlore (62%), quartz (9.6%), K-feldspar (5.1%), and kaolinite (1%).

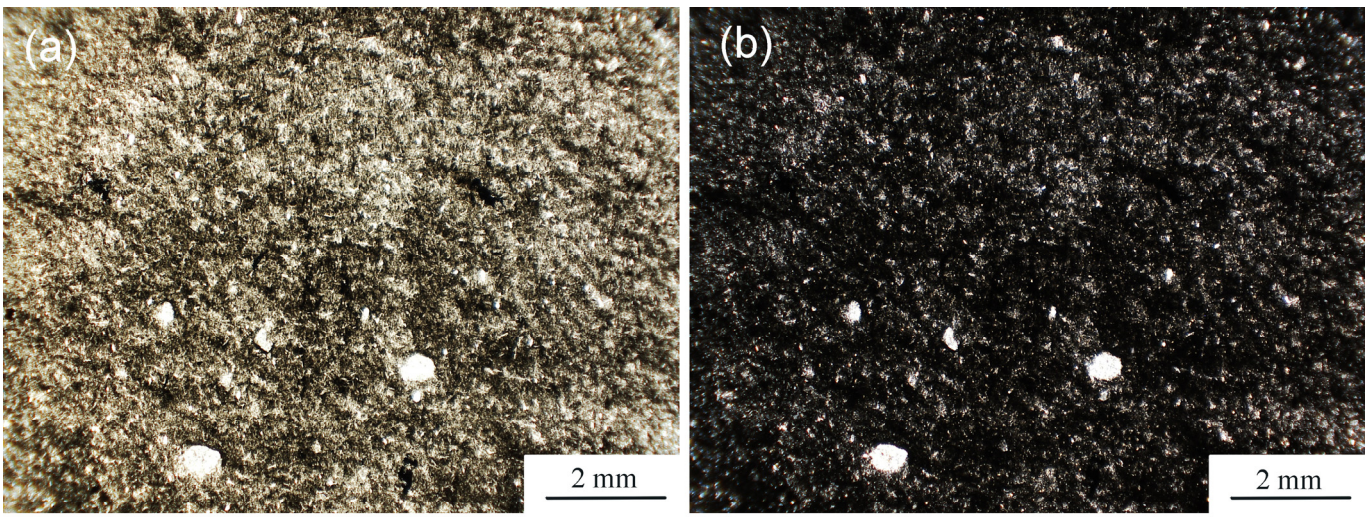


**Figure 3.** *Cont.*

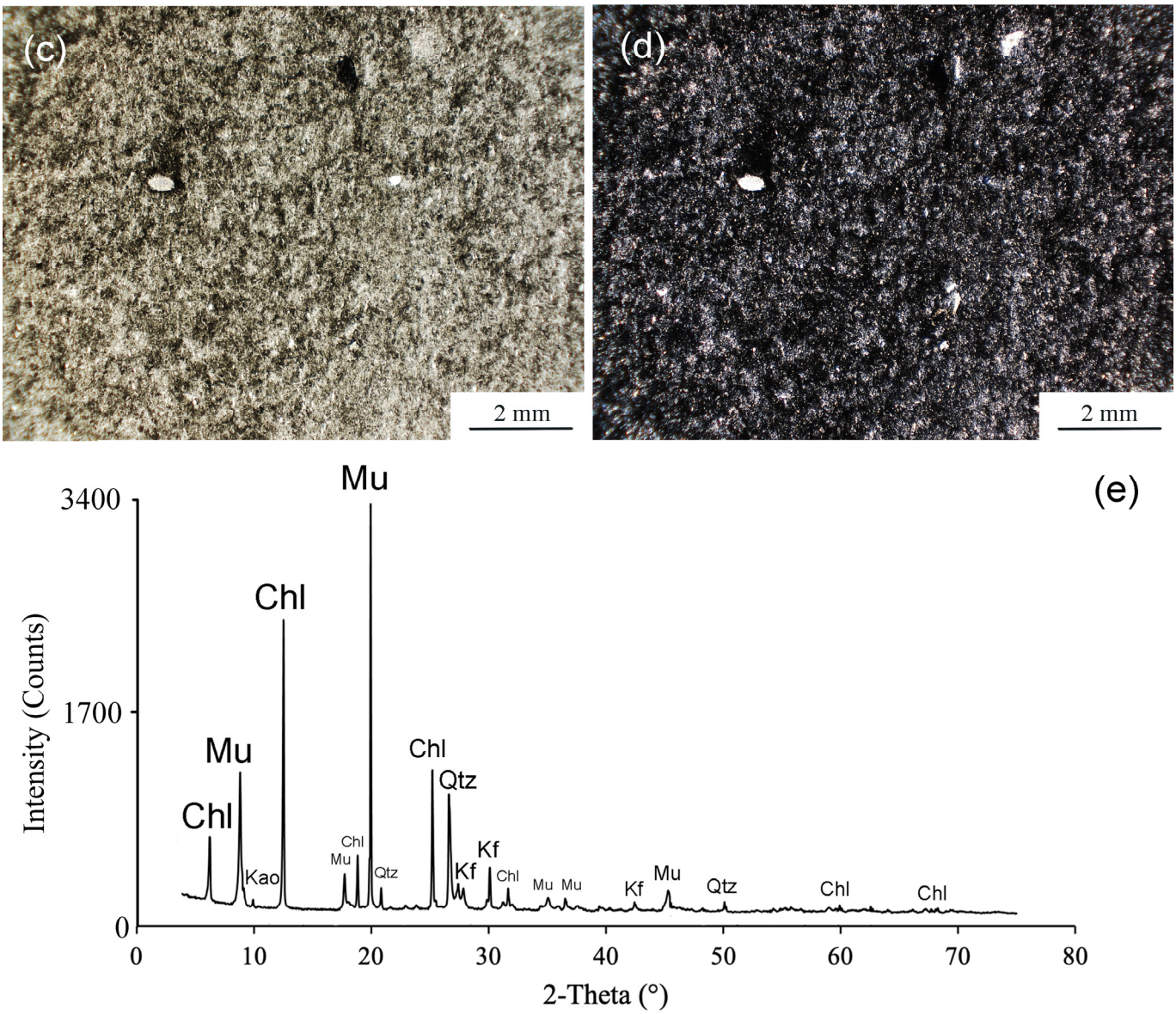


**Figure 3.** Petrography and mineralogy of the Valongo slate: (**a**) thin section parallel to cleavage (PPL); (**b**) thin section parallel to cleavage (NC); (**c**) thin section perpendicular to slaty cleavage (PPL); (**d**) thin section perpendicular to cleavage (NC); (**e**) semi-quantitative X-ray diffraction data with peaks corresponding to: Clinochlore (Chl, $(MgFe)_5Al(Si_3Al)O_{10}(OH)_8$), Muscovite (Mu, $KAl_2(AlSi_3O_{10})(F,OH)_2$), Kaolinite (Kao, $Al_2Si_2O_5(OH)_4$), Quartz (Qtz, $SiO_2$), Potassium feldspar (Kf, $KAlSi_3O_8$).

## 3. Materials and Methods

### *3.1. Materials*

All specimens were cut with a circular diamond saw and have a honed finishing. Dimension of specimens needed for the physical properties and mechanical behavior before and after the aging were:

(i) Prisms of 300 × 50 × 50 mm for flexural strength test (EN 12372, determination of flexure strength under concentrated load), measurement of sound propagation velocity (EN 14579, determination of sound speed propagation), and fundamental resonance frequency for the calculation of the elastic modulus (EN 14146, determination of dynamic elastic modulus);

(ii) Cubes of 50 × 50 × 50 mm for apparent density and open porosity (EN 1936, determination of the real and apparent density and of the total and open porosity),

water absorption test (EN 13755, determination of water absorption at atmospheric pressure), and uniaxial compression test (EN 1926, determination of uniaxial compressive strength);

(iii) Slab-anchored specimens with stainless-steel metallic pins of 200 × 200 × 30 mm. In this last set, slabs had a 10 mm hole with 30 mm depth located in the center of each side in which the metallic anchor was fixed with CEM I 52.5 R according to EN 13364 (determination of the breaking load at dowel hole) standard test method requirements. Slate anisotropy was considered for specimens used in the flexural, compression, anchor rupture load, and capillary rising tests, and the specimens were oriented perpendicular to bedding planes;

(iv) Prisms of 15 × 15 × 25 mm for the point load test (ASTM D 5731—determination of the point load strength index of rock);

(v) Prisms of 20 × 20 × 8 mm for the accelerated aging from sunlight exposure in the SOLARBOX chamber.

### 3.2. Methods

Stone paragenesis was identified through the analyses of 30 µm thin sections with the optical polarized microscope Leica DM2500P and a Hirox-01 microscope.

For the XRD analyses, a Bruker AXS D8 Discover XRD with a CuK$\alpha$ source, operating at 40 kV and 40 mA, and a Lynxeye 1-dimensional detector was used. Scans were performed from 3 to 75° 2θ, with 0.05° 2θ step, and 1 s/step measuring time by point. DiffractEva software from Bruker with PDF-2 mineralogical database (International Centre for Diffraction Data—ICDD) was used to identify the peaks.

Regarding physical characterization, before the tests, all specimens were dried in a ventilated oven at 70 ± 5 °C until constant mass was reached. After drying, specimens were left in the desiccator for cooling for approximately 8 h at room temperature.

Compressive strength ($\sigma_C$) was assessed by uniaxial compression test in accordance with the EN 1926 standard on cubic specimens (50 mm side) [43]. The equipment used was an EL200 hydraulic press by PEGASIL with 1200 kN range capacity, accuracy of 0.01 kN, and a load rate capacity of 1 ± 0.5 MPa/s. Load was applied perpendicular to the bedding planes.

Flexural strength ($\sigma_F$) tests under concentrated load were carried out in accordance with standard EN 12372 in a CEI-ZIPOR flexural press with a 25 kN load cell, an accuracy of 0.001 N, at a constant crosshead displacement speed of 0.25 ± 0.05 MPa/s until rupture [44]. Load was applied normal to the bedding planes.

Anchorage rupture load (ARL) tests were performed in accordance with standard EN 13364 in a CEI-ZIPOR press with a 25 kN load cell and an accuracy of 0.001 N [45]. Tests were carried out for the dowel–hole anchoring fixing system. Each slate slab had four drilled holes, one at each side, allowing four anchorage strength tests per slab in a total of twelve tests. Stainless-steel pins/dowels were placed and fixed inside the slate holes with CEM I 52.5 R after the specimens were completely dried and prior to placing the specimens in the climatic chamber.

Point load strength index normalized for a diametral test of 50 mm ($Is_{50}$) was determined with a point load tester (mod. Controls D550 Instrument) with a load capacity of 56 kN and accuracy of 50 N, following the test procedure described in ASTM D 5731 [46].

Measurements of the P-wave speed (Vp) were carried out using a PUNDIT PL200 PROCEQ tool with transducers of 54 kHz and an accuracy of 0.1 µs; all measurements were made according to EN 14579 standard and also perpendicular to the slaty cleavage [47].

Young's modulus was calculated according to the reference standard EN 14146, from the measurement of fundamental resonance frequency by the ERUDIY MKII resonant frequency test system in longitudinal mode, coupled with an oscilloscope, OS-9000SRS by GoldStar ("EN 14146—Natural stone test methods—Determination of the dynamic modulus of elasticity (by measuring the fundamental resonance frequency)" 2004) [48].

The apparent density ($\rho_B$) and open porosity ($\Phi$) tests were performed according to EN 1936 standard; each specimen was weighed and afterwards placed in a vacuum vessel where the pressure was gradually lowered until it reached approximately 2.0 ± 0.7 kPa (15 ± 5 mm Hg). Then, slowly, demineralized water was introduced into the vessel until the specimens were completely immersed. Once submerged, the vacuum was maintained for another 24 h. Afterwards, the pressure was changed to atmospheric, and specimens were left submerged in water at atmospheric pressure for more than 24 h. After 24 h, each soaked specimen was weighed in water and in air.

The mechanical tests: uniaxial compression, point load, and flexural strength have been measured with load application perpendicular to the slaty cleavage.

To measure the roughness on polished samples, a rugosimeter, MITUTOYO SURFTEST SJ-210, with a range of 0.001–10 µm and calibrated by standard ISO1997 was used. Roughness Ra value (arithmetic mean value of the deviations (taken in absolute value) of the real profile of the surface with respect to the mean line) was calculated according to the equation:

$$Ra = 1/L \int^{L}_{0} \mid Z(x) \mid dx$$

where L is the exploration length.

Color data were collected on the surface of the stone with a portable DataColor Check Plus II spectrophotometer with an accuracy of 0.01 and range of 0–100 using CIEL*a*b* color space.

#### 3.2.1. Artificial Climatic Cycles—FITOCLIMA Chamber Setting

Specimens were exposed to artificial climatic cycles in an ARALAB FITOCLIMA 500EC45 climatic chamber (temperature range of −45–180 °C, humidity range of 10–90%, and an accuracy of 0.1). The chamber was set up to reproduce four seasons of subpolar climatic conditions. Setting data were obtained from a regional meteorological station (Table 1). Slate specimens were exposed to one series of 30 days for each season following the order described in Table 2 (from winter to fall). Each season included controlled conditions of temperature and rainfall.

**Table 1.** Seasonal climatic data obtained from Livigno meteorological center (Italy) and selected for each season simulation in the climatic chamber ARALAB FITOCLIMA 500EC45.

| Season | Average Min. Temperature (°C) | Average Max. Temperature (°C) | Average Rainfall Accumulation (mm) |
|---|---|---|---|
| Winter | −12.6 | −4.2 | 362 |
| Spring | 0.9 | 6.7 | 723 |
| Summer | 5.9 | 13.1 | 581 |
| Autumn | −7.5 | −0.5 | 417 |

**Table 2.** Detailed description of the selected temperatures and steps for each season simulation in the climatic chamber ARALAB FITOCLIMA 500EC45.

| | Conditioning | Step (i) | Step (ii) | Step (iii) |
|---|---|---|---|---|
| Winter—repeated for 1 month | Soaking and rainfall for 1 h at 10 °C | 2 h \| −12.6 °C | 1:30 h \| −12.6 °C→−4.2 °C | 2:30 h \| −4.2 °C→−12.6 °C |
| Spring—repeated for 1 month | | 2 h \| 0.9 °C | 1:30 h \| 0.9 °C→−6.7 °C | 2:30 h \| 6.7 °C→0.9 °C |
| Summer—repeated for 1 month | | 2 h \| 5.9 °C | 1:30 h \| 5.9 °C→13.1 °C | 2:30 h \| 13.1 °C→5.9°C |
| Fall—repeated for 1 month | | 2 h \| −7.5 °C | 1:30 h \| −7.5 °C→−0.5 °C | 2:30 h \| −0.5 °C→−7.5 °C |

Each cycle consisted of 6 h exposure according to Table 2 and Figure 4. Each season simulation was automatically performed and consisted of a cycle repetition for 30 days that combined preliminary soaking and rainfall for 1 h at 10 °C at the beginning of each cycle. The conditioning step allowed soaking the slate specimens at the beginning of each cycle through the combined action of simulated rainfall and complete immersion of the samples.

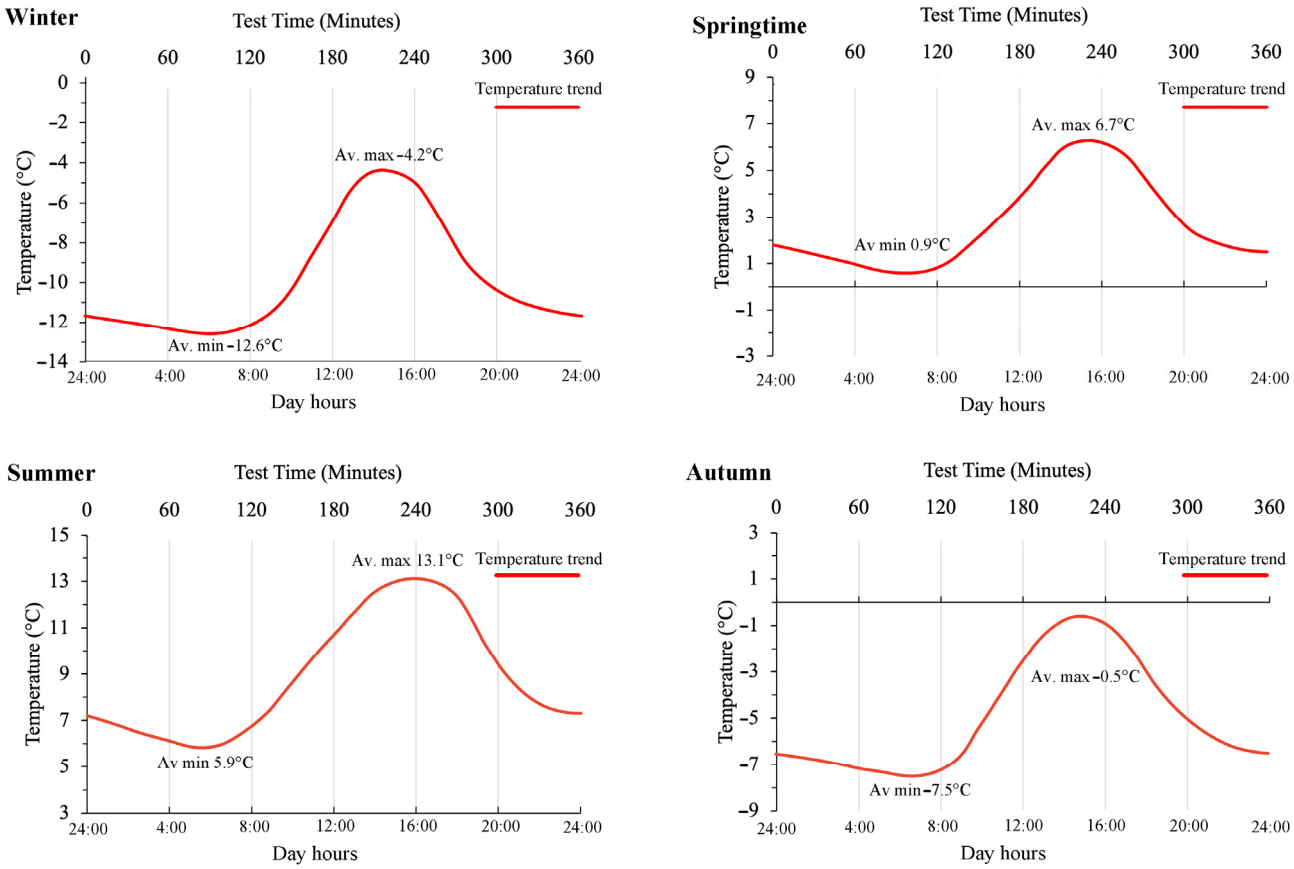


**Figure 4.** Climatic chamber cycle parameters set up for each season to artificially reproduce the subarctic climate Dfc.

The criteria to assess the simulated subarctic climate effect on slate were based on the EN 12371 recommended tests, with the addition of other relevant properties: (i) initial and final visual inspection (after the season simulation in the climatic chamber as described in Table 2); (ii) initial and final uniaxial compressive strength and flexural strength under concentrated load, anchor rupture load, point load strength index, P-wave ultrasound speed, Young's modulus, apparent density and open porosity, color, and roughness measurement.

In the last 15 min of the conditioning step, the water was drained, the rain stops, and the temperature started decreasing at a rate of approximately 2.8 °C/min until it reached the initial temperature of each season. The same temperature rate was used after step (iii) at every beginning of a new condition stage.

The cycle duration set by this experiment in the climatic chamber (6 h duration) allowed the samples to reach a uniform temperature including the interior, confirmed through continuous temperature monitoring with a mobile temperature sensor placed inside the thicker specimen used (50 mm thickness—prismatic specimens). Although this result has been achieved, many authors point out that the accelerated aging in the climatic chamber is not perfectly parallel to natural degradation [49].

This test should be validated in a real outdoor environment considering also the sunlight effect apart from thermal cycles. The sunlight effect will affect only one of the sides of the roofing slab, and this might lead to other contributions such as differential

thermal expansion between the exposed surface and the back of the slabs. The experiment should have a duration of one year or rather the hypothetical period of exposure simulated in the climatic chamber. Thus, the results obtained by natural aging can be compared with data obtained in the laboratory.

#### 3.2.2. Solar Radiation Simulation—SOLARBOX Chamber Setting

The solar radiation simulation was conducted with a SOLARBOX 1500 CO.FO.MEGRA chamber equipped with a 295–800 nm UV outdoor filter. Specimens underwent 1 month of testing with a fixed value of solar radiation of 1000 W/m$^2$ (equipment range of 100–1000 W/m$^2$).

During SOLARBOX aging, the solar irradiance was reproduced, and a relation between test time ($T_T$) and hypothetical outdoor exposure ($T_A$) was defined. The test time ($T_T$) is the period in which the specimens are placed in the climatic chamber. In this study, the experiments were conducted with $T_T$ = 1 month. The hypothetical outdoor exposure ($T_A$) is the time defined by the product of test time and a hypothetical acceleration factor. The term "hypothetical" means that the reproduction of the outdoor exposure on a climatic chamber is uncertain. This is because it is always recommended to test aging in a natural environment in order to verify the reliability of the artificial aging [50].

As for the FITOCLIMA setting, the meteorological data of the Italian Alpine region affected by Dfc climate were chosen in terms of average global solar radiation. The Alpine Dfc areas present an average annual global solar radiation variable between 4200 and 4700 MJ/m$^2$/year [51]. It is important to underline how this range of values is independent of the type of climate but is mainly linked to the latitude. A value of 4500 MJ/m$^2$/year has been selected as reference for our test corresponding to 12.33 MJ/m$^2$/day.

Only 6% of this radiation falls in the ultraviolet region between 295 nm and 400 nm, or rather the wavelengths that create the most damage to materials' surfaces.

A further correction of 67% is recommended and could be applied to allow the fact that not all this radiation is acting at higher summer temperatures, and so it will be less damaging to the affected surfaces [52]. This means that the Alpine Dfc area records a solar radiation of 12.33 MJ/m$^2$/day × 0.06 × 0.67 = 0.49 MJ/m$^2$/day 295–400 nm.

The average daily solar radiation of the international standard place (Miami, FL, USA) is 1 MJ/m$^2$/day 295–400nm [53]. Therefore, average daily radiation in Miami is (1 MJ/m$^2$/ day 295–400 nm/0.49 MJ/m$^2$/day 295–400 nm) = 2.04 times the average daily radiation of Alpine Dfc areas. In this research, a radiation of 1000 W/m$^2$ was selected in the SOLARBOX.

According to the SOLARBOX manufacturer, the chamber set at 1000 W/m$^2$ with a 295–800 nm UV outdoor filter for one day of testing ($T_T$ = 1 day) reproduces 9.60 MJ/m$^2$ 295–400 nm, corresponding to 9.6 days ($T_A$ = 9.6 days) of hypothetical outdoor exposure in Miami and 9.6 days × 2.04 = 19.6 days ($T_A$ = 19.6 days) in Alpine Dfc areas. Therefore, the relation $T_T$–$T_A$ for Alpine Dfc areas is:

$$TA = F \times T_T \text{ (1000 W/m}^2 \text{ with 295-800 nm UV outdoor filter)}$$

where F is the acceleration factor = 19.6.

It is essential to underline that the high temperature registered inside the SOLARBOX, as indicated by the manufacturer CO.FO.MEGRA, can accelerate the aging speed. During our experiments, the temperature inside the SOLARBOX was always in the range of 30 < T < 40 °C.

Considering a period of test duration $T_T$ = 1 month, with a radiation of 1000 W/m$^2$, the hypothetical solar outdoor exposure for a slate sample in the Alpine Dfc area is $T_A$ = 19.6 months.

## 4. Results and Discussion

Visual observations after the four-season simulation in the FITOCLIMA climatic chamber showed no changes in appearance regarding any discoloration due to oxidation of metallic minerals and inclusions.

The physical and mechanical properties before and after the aging are listed in Table 3. As introduced in the above sections, the subarctic Dfc climate can cause deep damage in most artificial and natural materials including natural stones. According to the decay diagram [54] and based on the mean annual precipitation (2085 mm) and temperature (0.2 °C), the weathering conditions on geomaterials of Dfc Alpine sectors are not specified. However, the chemical decay (e.g., dissolution, hydration, hydrolysis oxidation, and reduction) and the biological decay (e.g., wedge work of roots and burrowing and boring of animals) is lower at average annual temperatures around zero or less, and in fact in this research no chemical degradation was detected. Conversely, physical decay, in particular the frost action, was naturally higher. The effects of freeze–thaw action are linked to pore space and pore size distribution in stones (open porosity of >5%). However, damage is also reported in low-porosity stone materials such as marbles, granites, and slates. In these stones, damage can be related to other textural features (besides the characteristics of the pore space) such as the presence of slaty cleavage planes, veins, or stylolites [55].

**Table 3.** Physical–mechanical properties of the slate selected to assess the impact of subarctic climatic conditions through seasonal cycles with a total length of four months.

| Physical and Mechanical Properties | No. of Tested Specimens | Before Aging | After Aging | Relative Difference (%) |
|---|---|---|---|---|
| Uniaxial compressive strength (MPa) | 10 | 175 ± 13 | 133 ± 14 | −24 |
| Flexural strength under concentrated load (MPa) | 10 | 30.4 ± 9.2 | 14.9 ± 3.8 | −50.9 |
| Anchor rupture load (N) | 12 × 4 | 3141 ± 221 | 2420 ± 275 | −22.9 |
| Point load strength index (MPa) | 10 | 13.1 ± 3.1 | 12.5 ± 2.4 | −4.5 |
| P-wave ultrasound speed (m/s) | 10 | 6120 ± 410 | 5566 ± 146 | −9 |
| Young's modulus (GPa) | 10 | 88.5 ± 13.1 | 72.3 ± 6.9 | −18.3 |
| Apparent density (kg/m$^3$) | 6 | 2833.5 ± 6.5 | 2813.4 ± 3.8 | −0.7 |
| Open porosity (%) | 6 | 0.87 ± 0.1 | 1.5 ± 0.2 | 72 |

A similar type of damage was recorded in this study's aging cycles, as the crystallization of water inside the slate caused major longitudinal fractures, S1 parallel to S0 slaty cleavage planes, visible in Figure 5. These fractures have openings varying between 50 and 150 µm with irregular spacing in the order of 5 cm (Figure 6a,c). Moreover, principles of exfoliation and spalling are present in the samples following exposure to seasonal cycles (Figure 6b,d). From Table 3, it is seen that the volumetric expansion caused an increase in the porosity of the slate from a pre-aging value of 0.87 ± 0.1 to 1.5 ± 0.2%, indicating an increase of 72%. Similarly to the information reported [56], this change in porosity was caused by microfissures, some small amounts of debris, and some slaty cleavage planes' partial and total detachment.

An irrelevant change in the apparent density was detected (−0.7%), shifting from 2833.5 ± 6.5 kg/m$^3$ to a final value of 2813.4 ± 3.8 kg/m$^3$, as shown in Table 3. The increase in the porosity due to the opening of the fracturing planes causes a lower speed of propagation of the compressional P-wave. The initial value of 6120 ± 410 m/s was reduced by approximately 9 %, to 5566 ± 146 m/s. Following the aging test, the values of VRI (Velocity Ratio Quality Index) [57] were assessed as 0.91 < VRI < 0.97. This parameter

indicates the stone quality based on the ultrasonic velocity measurements before ($V_{pre}$) and after the aging ($V_{post}$).

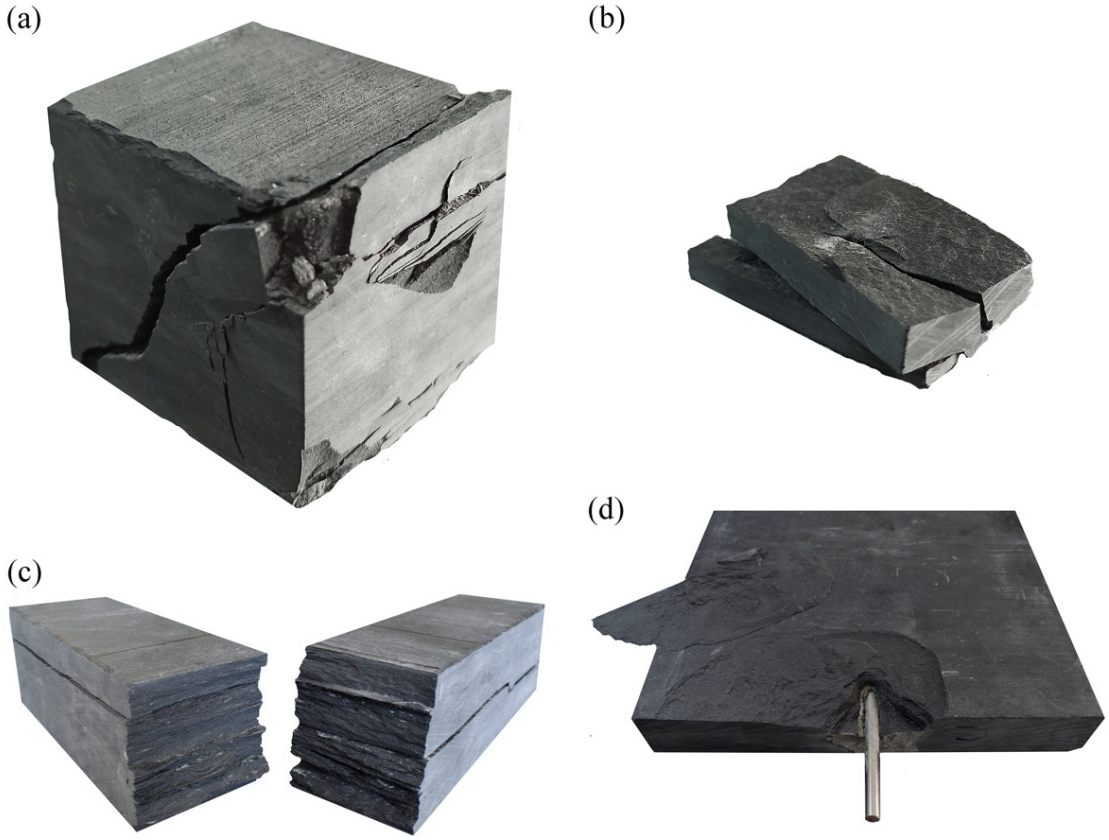


**Figure 5.** Results of aging test and mechanical characterization: (**a**) cubic slate, 50 mm side—rupture after uniaxial compression test; (**b**) prismatic specimens, 15 × 15 × 25 mm—rupture after the determination of point load strength index; (**c**) prismatic slate specimens, 50 × 50 × 300 mm dimensions—rupture after flexure test; (**d**) slate specimens, 200 × 200 × 30 mm dimensions—rupture after the anchorage test.

VRI was calculated as $(V_{post}/V_{pre})^{0.5}$. These VRI values indicate a "very good" QBM (Quality of Building Materials). A classification of "very good" means that, in terms of ultrasonic speed, the samples withstood the accelerated degradation test excellently, meaning that freeze–thaw decay mainly affected the external part of the specimens, leaving the core relatively intact.

The compressive strength of the material, and the point load index, suffered a significant decrease from 175 ± 13 MPa to 133 ± 14 MPa and 13.1 ± 3.1 MPa to 12.5 ± 2.4 MPa (24 and 4.5% change, respectively). The difference between the decay determined by the two methods is intrinsically linked to the test specification: (i) the uniaxial compression test uses a load applied uniformly to the specimen (50 mm side), and all the bulk (interior and exterior) contributes in a much more effective way to strength. Moreover, there is a higher probability of finding a critical defect that causes rupture [58,59]. (ii) Conversely, in the point load test, the load is applied to one point (located in the central area of the specimen), and there is a lower contribution of the decayed external part of the sample. In this method, the results are expected to present a lower change after the accelerated degradation test. In a realistic situation, the achieved results will create a structural weakening. Over time outdoors, the stone decreases its compressive strength due to microfracturing caused by frost effect.

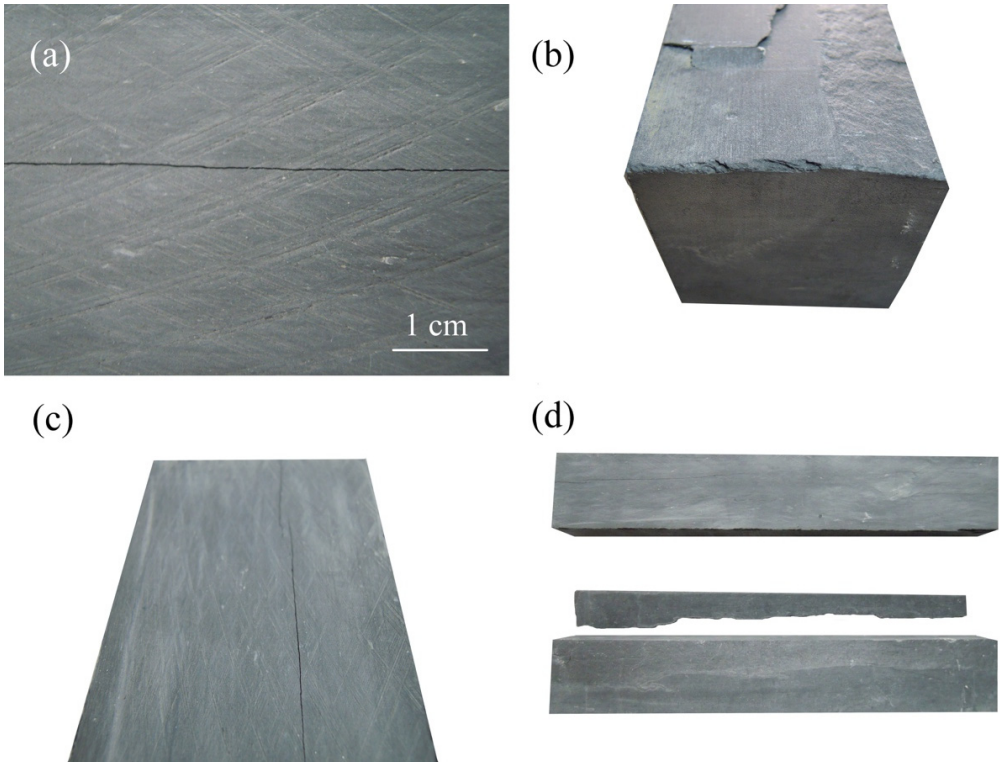


**Figure 6.** Slate damaging after aging: (**a**,**c**) S1 fractures due to volumetric expansion of the ice oriented parallel to the S0 slaty cleavage; (**b**,**d**) decay by spalling and exfoliation.

As seen in Figure 5a, the cubic specimens (tested for uniaxial compressive strength) broke according to fracturing systems consistently oriented about 45°. In the point load test and in the flexure strength test (Figure 5b,c), the samples broke based on two fracturing systems, perpendicular and parallel to the load application.

The flexural strength of the samples is again conditioned by the S1 fracturing system and by the slaty cleavage itself, considering that the prisms tested cannot be the same before and after the aging. During the application of the load, the sliding of the upper and lower portions occurs along these fractures. This behavior is like a car leaf spring. The fractures favor a ductile behavior of the specimen during the flexural test, probably increasing its flexural curvature but simultaneously reducing the flexural strength. In fact, flexural strength changed from an initial value of 30.4 ± 9.2 to 14.9 ± 3.8 MPa, reaching a total decrease of −50.9 % (Table 2).

Fractures (S1) due to frost are once again responsible for the decrease in the anchorage strength. In this test, the load was in fact perpendicularly applied to the slaty cleavage planes and tends to widen the planes by increasing their opening (Figure 6a,c). The results showed a relevant change from the anchorage rupture load, from 3141 ± 221 N in pre-test to 2420 ± 275 N.

The solar simulation in the FITOCLIMA climatic chamber resulted in no relevant change in color.

Figure 7a shows rather constant trends of the parameters L, a and b, although characterized by normal fluctuations [60]. The color difference parameter ΔE has values between 2.34 and 0.45, and in any case always lower than the JND (just noticeable difference = 2.37), the minimum value that the human eye can perceive (Figure 7b).

It is important to underline how the color changes of the slates certainly depends on various factors.

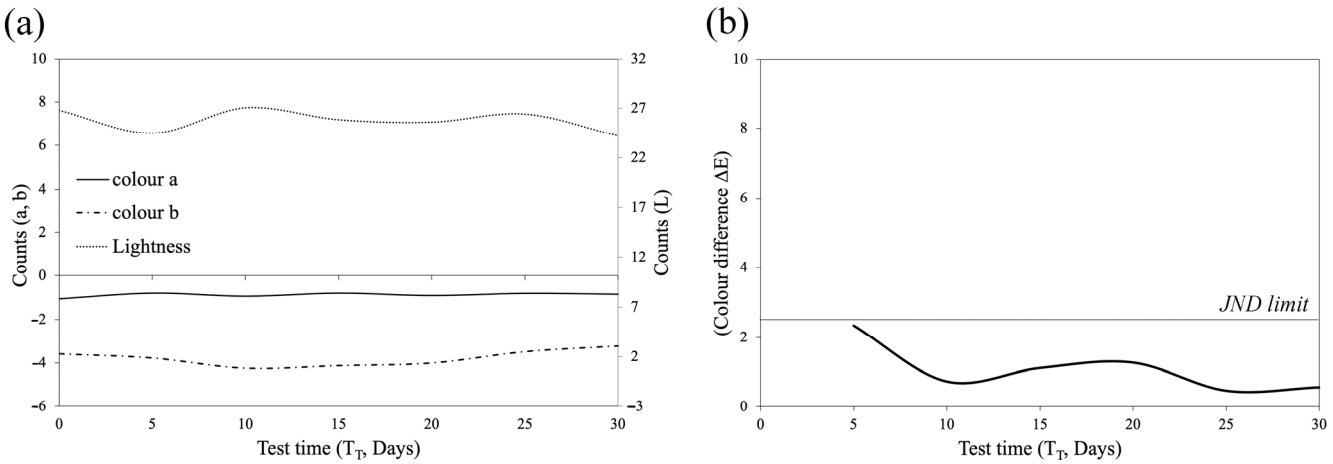


**Figure 7.** (**a**) Trends of CIEL*a*b* color parameters during 30 days of solar exposure test; (**b**) color difference according to the JND limit (just noticeable difference = 2.37).

Slates can be affected by the weathering of the iron sulphides (mainly pyrite $FeS_2$ and pyrrhotite $Fe_{1-X}S$, $0 < X < 0.2$) that the stone may contain. This can lead to the formation of brown/yellow/red iron crust compounds (Figure 8a,d) bearing limonite ($2Fe_2O_3 \cdot 3H_2O$) and goethite (FeO(OH)). The fading toward white could be linked to sulphation of the carbonates to gypsum or Na-sulphates. In this regard, we note that calcite ($CaCO_3$) could be present in the slate.

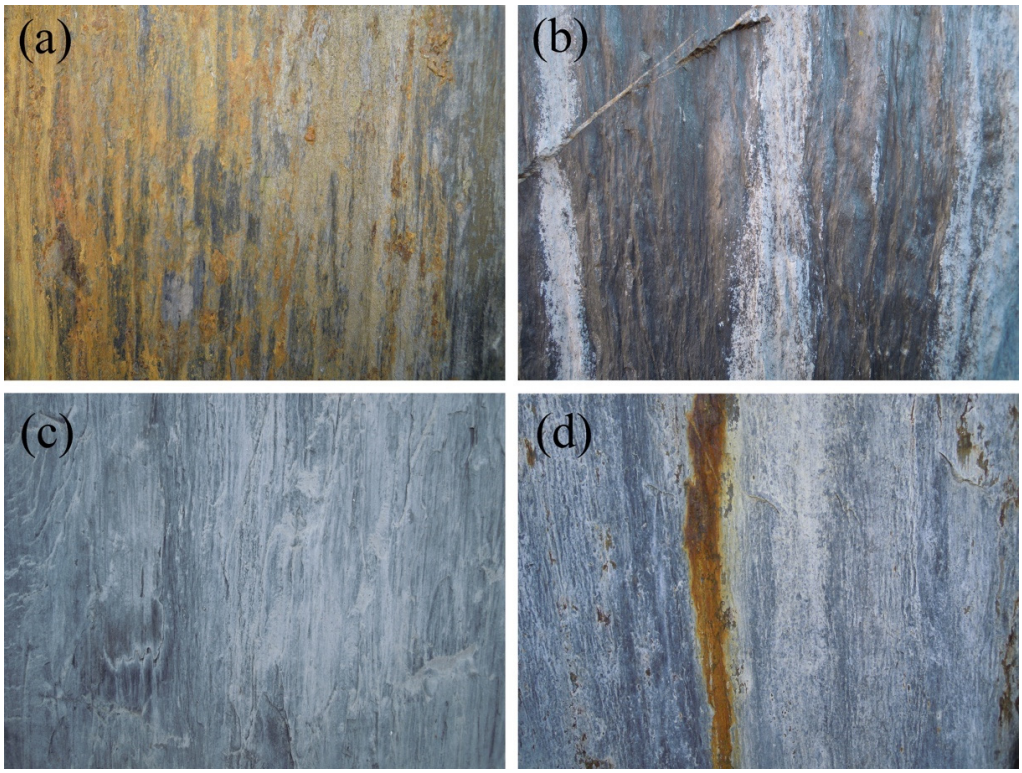


**Figure 8.** Color change of slate slabs: (**a**) oxidation; (**b**) deposition corresponding to water runoff; (**c**) dirty deposition of cement grouts; (**d**) oxidation. Photo credits by Fabio Sitzia.

In some cases, white stains could derive from adhesives and/or cements used to install slate slabs in floors or claddings (Figure 8c). The presence of white depositions is also identified as corresponding to water runoff (Figure 8b,d).

Furthermore, the type of finish and therefore the roughness of the stone is closely linked to the color, as shown in Figure 9. As detailed in these pictures, the greater the surface roughness (Ra), the whiter the color of the slate. In this regard, we highlight that in polished slate surfaces and in carbonate rocks exposed to rain and frost cycles, there may be a decrease in gloss linked to microcorrosion and therefore an increase in roughness [22,61]. In Figure 9, in fact, a fading towards white is detected by Ra feature increases.

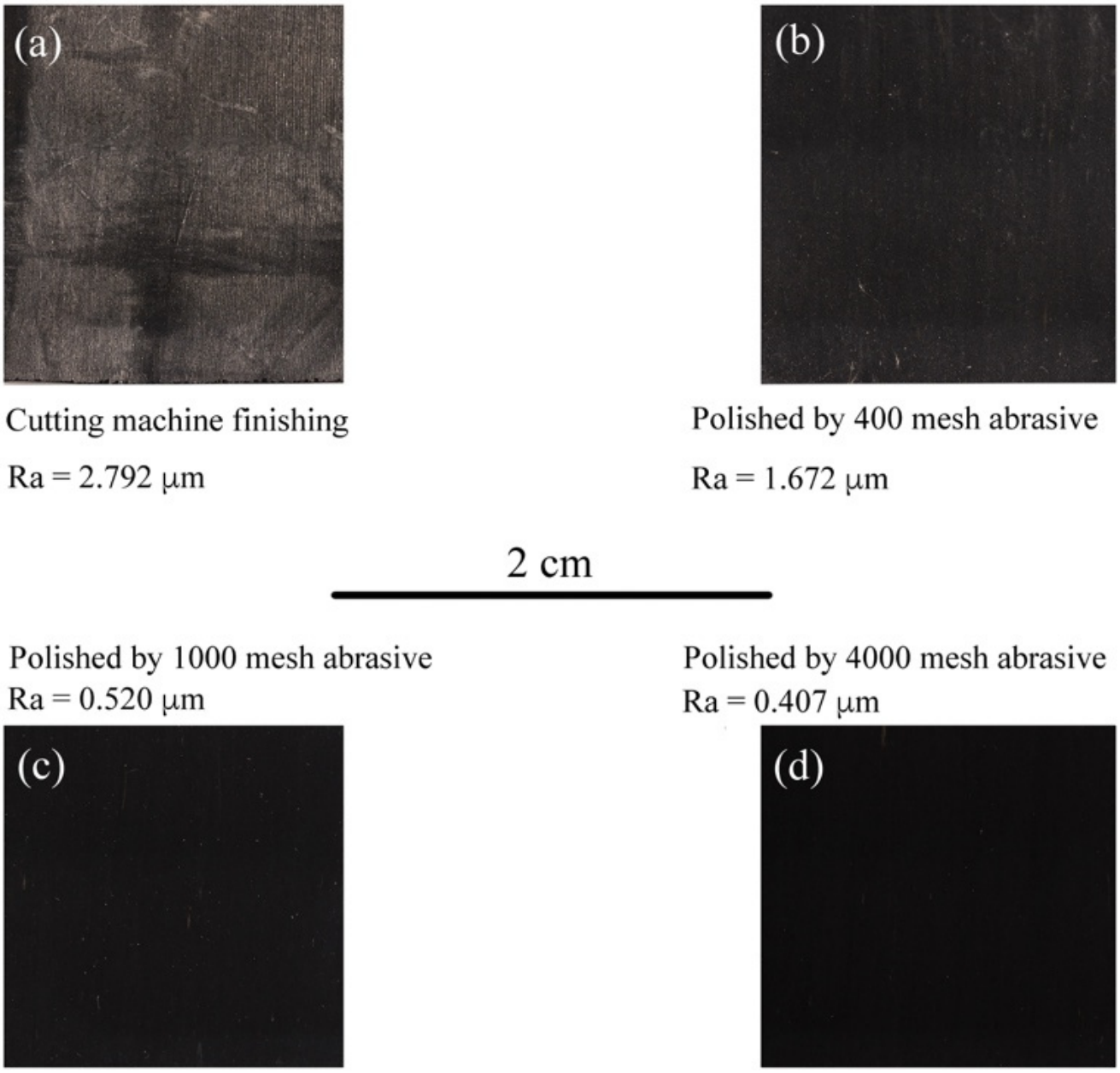


**Figure 9.** Correlation between color and roughness of the slate: a lower roughness (Ra) corresponds to a darker color with a progressive decreasing of L* parameter. (**a**) Cutting machine finishing; (**b**) polishing by FEPA P400-mesh abrasive (35 mm, 0.0014″); (**c**) polishing by FEPA P1000-mesh abrasive (18.3 mm, 0.007″); (**d**) polishing by FEPA P4000-mesh abrasive (5 mm, 0.0002″).

## 5. Conclusions

Slates are common building stones that are used as roof coverings and cladding because of their physical properties and mechanical performance making them suitable for

application in cold climates. Slates represent a typical example of the use of traditional raw materials in vernacular architecture like many other common stones.

In this paper, the results of a laboratory simulation of subarctic climate, carried out in a climatic chamber, are presented with the aim of strengthening the awareness of material quality and frost engineering performance. The setting data for the simulation were obtained from a local meteorological station, and cycles consisted of accelerated reproduction of the seasons automatically lasting 30 days each. Chamber settings starting with realistic meteorological data are scarce in the literature and represent an innovative procedure of a reliable freezing–thawing experiment.

The test results reveal a predominant degradation with different alterations due to freeze–thaw intra-fracturing: (i) relevant changes in compressive strength, flexural strength, and open porosity; (ii) moderate reduction in anchor rupture load and Young's modulus; (iii) relative lowering of P-wave velocity and point load strength index; (iv) no relevant changes in apparent density and water absorption; and (vi) absence of chemical-mineralogical alteration.

Physical mechanical data show how the loss in performance of the slate is relatively fast.

In only one year of hypothetical outdoor exposure aging, we registered a worsening of some parameters from 9 to about 50%. In particular, after this test, one of the most susceptible parameters to frost deterioration was the flexural strength. In this sense, architectural elements such as architraves, facades, or balconies must be frequently monitored. Given the achieved level of loss in flexural strength, it is recommended that slate elements should be monitored and reinforced or replaced to avoid risks for users. Moreover, the compressive strength of the rock suffered frost damage with a loss of about −24% in the performance.

In the sun exposure test, no substantial changes in the color of the slate were identified. This basically debunks the belief that slate can lighten following exposure to the sun.

The purpose of our study was to perform a laboratory simulation that could help anticipate the behavior of the stone material in a specific climate category. The improvement of natural stone selection processes in construction projects is crucial today, especially in cold regions.

However, nowadays, confirming the validity of an aging test by comparing it to an outdoor environment is needed. This could be performed in future studies by placing the samples outdoors in a Dfc area and verifying whether the relative percentage and color differences obtained in the climatic chamber are the same or close to those obtained outdoors. This will be carried out in future studies aiming to understand the real behavior of materials in order to optimize production processes and the dimensioning of cladding and roofing elements.

**Author Contributions:** Conceptualization, F.S., V.P. and C.L; methodology, F.S., V.P. and C.L.; software, F.S., V.P., C.L. and T.A.; validation, F.S., V.P., C.L. and J.M.; formal analysis, F.S., V.P., C.L. and T.A.; investigation, F.S., V.P., C.L. and J.M.; resources, J.M.; data curation, F.S., V.P. and C.L.; writing—original draft preparation, F.S.; writing—review and editing, F.S., V.P. and C.L.; visualization, J.M.; supervision, F.S.; project administration, F.S.; funding acquisition, F.S., V.P., C.L. and J.M. All authors have read and agreed to the published version of the manuscript.

**Funding:** The authors gratefully acknowledge the following funding sources: INOVSTONE4.0 (POCI-01-0247-FEDER-024535), co-financed by the European Union through the European Regional Development Fund (FEDER) and Fundação para a Ciência e Tecnologia (FCT) under the project UID/Multi/04449/2013 (POCI-01-0145-FEDER-007649), and Fundacao para a Ciencia e Tecnologia (FCT) under the project UIDB/04449/2020 and UIDP/04449/2020. The authors gratefully acknowledge the European Communion—Portugal, Grant Contract number: Sustainable Stone by Portugal Call: 2021-C05i0101-02—agendas/alianças mobilizadoras para a reindustrialização—PRR, Proposal: C632482988-00467016.

**Institutional Review Board Statement:** Not applicable.

**Informed Consent Statement:** Not applicable.

**Data Availability Statement:** Not applicable.

**Conflicts of Interest:** The authors declare no conflict of interest.

## References


1. Geiger, R. Classificação Climática de Köppen- Geiger. *Creat. Commons Attrib. Alike 3.0 Unported 1936*. Available online: https://www.google.com/url?sa=i&rct=j&q=&esrc=s&source=web&cd=&ved=0CAQQw7AJahcKEwjIt8GisKT9AhUAAAAAHQAAAAAQAg&url=http%3A%2F%2Fwww.pha.poli.usp.br%2FLeArq.aspx%3Fid_arq%3D24064&psig=AOvVaw0Am1xDXGGkTQapStaHRXTo&ust=1676992005714690 (accessed on 10 February 2023).
2. Beck, H.E.; Zimmermann, N.E.; McVicar, T.R.; Vergopolan, N.; Berg, A.; Wood, E.F. Present and Future Köppen-Geiger Climate Classification Maps at 1-Km Resolution. *Sci. Data* **2018**, *5*, 180214. [CrossRef] [PubMed]
3. Pinna, M. *L'atmosfera e Il Clima*; UTET: Torino, Italy, 1978.
4. Rubel, F.; Brugger, K.; Haslinger, K.; Auer, I. The Climate of the European Alps: Shift of Very High Resolution Köppen-Geiger Climate Zones 1800-2100. *Meteorol. Z.* **2017**, *26*, 115–125. [CrossRef]
5. Stern, P. *Critical Inuit Studies: An Anthology of Contemporary Arctic Ethnography*; University of Nebraska: Lincoln, NE, USA, 2006; ISBN 9780803293489.
6. Sitzia, F. Climate Change and Cultural Heritage: From Small- to Large-Scale Effects—The Case Study of Nora (Sardinia, Italy). *Heritage* **2022**, *5*, 3495–3514. [CrossRef]
7. Columbu, S.; Palomba, M.; Sitzia, F.; Carcangiu, G.; Meloni, P. Pyroclastic Stones as Building Materials in Medieval Romanesque Architecture of Sardinia (Italy): Chemical-Physical Features of Rocks and Associated Alterations. *Int. J. Archit. Herit.* **2020**, *16*, 49–66. [CrossRef]
8. García-Guinea, J.; Lombardero, M.; Roberts, B.; Taboada, J.; Peto, A. Mineralogy and Microstructure of Roofing Slate: Thermo-Optical Behaviour and Fissility. *Mater. Constr.* **1998**, *48*, 37–48. [CrossRef]
9. Lisci, C.; Sitzia, F. *Degrado, Danni e Difetti Delle Pietre Naturali e Dei Laterizi. Meccanismi Di Alterazione, Patologie, Tecniche Diagnostiche e Scehde Pratiche*; Maggioli: Santarcangelo di Romagna, Italy, 2021; ISBN 8891650351.
10. Martins, L.; Vasconcelos, G.; Lourenço, P.B.; Palha, C. Influence of the Freeze-Thaw Cycles on the Physical and Mechanical Properties of Granites. *J. Mater. Civ. Eng.* **2016**, *28*, 04015201. [CrossRef]
11. Thomachot, C.; Jeannette, D. Evolution of the Petrophysical Properties of Two Types of Alsatian Sandstone Subjected to Simulated Freeze-Thaw Conditions. *Geol. Soc. Spec. Publ.* **2002**, *205*, 19–32. [CrossRef]
12. Martínez-Martínez, J.; Benavente, D.; Gomez-Heras, M.; Marco-Castaño, L.; García-del-Cura, M.Á. Non-Linear Decay of Building Stones during Freeze–Thaw Weathering Processes. *Constr. Build. Mater.* **2013**, *38*, 443–454. [CrossRef]
13. Laskaridis, K.; Arapakou, A.; Patronis, M.; Kouseris, I. Correlations between the Physical Mechanical Properties of Greek Dimension Stones. *Mater. Proc.* **2021**, *5*, 28.
14. Park, K.; Kim, K.; Lee, K.; Kim, D. Analysis of Effects of Rock Physical Properties Changes from Freeze-Thaw Weathering in Ny-Ålesund Region: Part 1—Experimental Study. *Appl. Sci.* **2020**, *10*, 1707. [CrossRef]
15. Zhang, C.; Jin, X.; Hou, C.; He, J. Mechanical and Acoustic Emission Characteristics of Anhydrite Rock under Freeze-Thaw Cycles. *J. Mt. Sci.* **2023**, *20*, 227–241. [CrossRef]
16. Abdolghanizadeh, K.; Hosseini, M.; Saghafiyazdi, M. Effect of Freezing Temperature and Number of Freeze–Thaw Cycles on Mode I and Mode II Fracture Toughness of Sandstone. *Theor. Appl. Fract. Mech.* **2020**, *105*, 102428. [CrossRef]
17. Weng, L.; Wu, Z.; Taheri, A.; Liu, Q.; Lu, H. Deterioration of Dynamic Mechanical Properties of Granite Due to Freeze-Thaw Weathering: Considering the Effects of Moisture Conditions. *Cold Reg. Sci. Technol.* **2020**, *176*, 103092. [CrossRef]
18. Navarro, R.; Catarino, L.; Pereira, D.; Paulo, F.; Campos, D.S. Effect of UV Radiation on Chromatic Parameters in Serpentinites Used as Dimension Stones. *Bull. Eng. Geol. Environ.* **2019**, *78*, 5345–5355. [CrossRef]
19. Sitzia, F.; Lisci, C.; Mirão, J. Accelerate Ageing on Building Stone Materials by Simulating Daily, Seasonal Thermo-Hygrometric Conditions and Solar Radiation of Csa Mediterranean Climate. *Constr. Build. Mater.* **2021**, *266*, 121009. [CrossRef]
20. Atalaya, M. Preventive Conservation Applied to the Mineralogical Collection of the National Museum of Natural History and Science of the University of Lisbon. Ph.D. Thesis, Universidade Nova de Lisboa, Lisboa, Portugal, 2020.
21. Sitzia, F.; Lisci, C.; Mirão, J. Building Pathology and Environment: Weathering and Decay of Stone Construction Materials Subjected to a Csa Mediterranean Climate Laboratory Simulation. *Constr. Build. Mater.* **2021**, *300*, 124311. [CrossRef]
22. Sitzia, F.; Lisci, C.; Mirão, J. The Interaction between Rainwater and Polished Building Stones for Flooring and Cladding—Implications in Architecture. *J. Build. Eng.* **2022**, *52*, 104495. [CrossRef]
23. Labus, M.; Bochen, J. Sandstone Degradation: An Experimental Study of Accelerated Weathering. *Environ. Earth Sci.* **2012**, *67*, 2027–2042. [CrossRef]
24. Pires, V.; Amaral, P.M.; Rosa, L.G.; Camposinhos, R.S. Slate Flexural and Anchorage Strength Considerations in Cladding Design. *Constr. Build. Mater.* **2011**, *25*, 3966–3971. [CrossRef]
25. Taheri, B.M.; Ramezanianpour, A.M.; Sabokpa, S.; Gapele, M. Experimental Evaluation of Freeze-Thaw Durability of Pervious Concrete. *J. Build. Eng.* **2021**, *33*, 101617. [CrossRef]
26. Sitzia, F.; Peters, M.J.H.; Lisci, C. Climate Change and Its Outcome on the Archaeological Areas and Their Building Materials. The Case Study of Tharros (Italy). *Digit. Appl. Archaeol. Cult. Herit.* **2022**, *25*, e00226. [CrossRef]

27. Sitzia, F. The San Saturnino Basilica (Cagliari, Italy): An Up-Close Investigation about the Archaeological Stratigraphy of Mortars from the Roman to the Middle Ages. *Heritage* **2021**, *4*, 1836–1853. [CrossRef]
28. Ruedrich, J.; Kirchner, D.; Siegesmund, S. Physical Weathering of Building Stones Induced by Freeze–Thaw Action: A Laboratory Long-Term Study. *Environ. Earth Sci.* **2011**, *63*, 1573–1586. [CrossRef]
29. Lisci, C.; Pires, V.; Sitzia, F.; Mirão, J. Limestones Durability Study on Salt Crystallisation: An Integrated Approach. *Case Stud. Constr. Mater.* **2022**, *17*, e01572. [CrossRef]
30. Pires, V.; Rosa, L.G.; Amaral, P.M.; Simão, J.A.R. The Susceptibility to Salt Fog Degradation of Stone Cladding Materials: A Laboratory Case Study on Two Limestones from Portugal. *Heritage* **2023**, *6*, 492–504. [CrossRef]
31. Rivas, T.; Matías, J.M.; Taboada, J.; Argüelles, A. Application of Bayesian Networks to the Evaluation of Roofing Slate Quality. *Eng. Geol.* **2007**, *94*, 27–37. [CrossRef]
32. Molina, E.; Cultrone, G.; Sebastián, E.; Alonso, F.J. Evaluation of Stone Durability Using a Combination of Ultrasound, Mechanical and Accelerated Aging Tests. *J. Geophys. Eng.* **2013**, *10*, 035003. [CrossRef]
33. Amaral, P.M.; Fernandes, J.C.; Pires, V.; Rosa, L.G. Ornamental Stones. In *Materials for Construction and Civil Engineering*; Springer International Publishing: Cham, Switzerland, 2015; pp. 397–445.
34. Savioli, L. *Ardesia, Materia e Cultura*; Sagep: Genova, Italy, 1988.
35. Cardenes, V.; Cnudde, V.; Cnudde, J.P. Iberian Roofing Slate as a Global Heritage Stone Province Resource. *Episodes* **2015**, *38*, 97–105. [CrossRef]
36. Kenneth, H. *Building Materials*; Longman Group: London, UK, 1972; ISBN 0-582-12791-2.
37. Born, A. Blue Slate Quarrying in South Devon: An Ancient Industry. *Ind. Archaeol. Rev.* **2012**. [CrossRef]
38. Jope, E.M.; Dunning, G.C. The Use of Blue Slate for Roofing in Medieval England. *Antiq. J.* **1954**, *34*, 209–217. [CrossRef]
39. Leite, A.; Guedes, C. Louseiras De Valongo 2022. Available online: https://repositorio-aberto.up.pt/bitstream/10216/141561/2/565602.pdf (accessed on 10 February 2023).
40. Bartels, C.; Briggs, D.E.G.; Brassel, G. The Fossil Record of the Hunsrück Slate: Marine Life in the Devonian. *Palaeontol. Electron.* **1999**.
41. Hagen, A. *Norges Oldtid*; Cappelen: Oslo, Norway, 1967; ISBN 82-02-09067-9.
42. Delgado, N.; Choffat, P. (Eds.) *Carta Geológica de Portugal, Escala 1:500000*; Direcção dos Trabalhos Geológicos: Lisbon, Portugal, 1908.
43. EN 1926:2006—Natural Stone Test Methods—Determination of Uniaxial Compressive Strength. Available online: https://standards.iteh.ai/catalog/standards/cen/227bc05a-f18c-474f-8178-fd6f613fe740/en-1926-2006 (accessed on 9 August 2022).
44. EN 12372:2006—Natural Stone Test Methods—Determination of Flexural Strength under Concentrated. Available online: https://standards.iteh.ai/catalog/standards/cen/304e13c4-a1ea-4a80-af45-ce1a644b5316/en-12372-2006 (accessed on 9 August 2022).
45. EN 13364—Natural Stone Test Methods—Determination of the Breaking Load at Dowel Hole. Available online: https://standards.iteh.ai/catalog/standards/cen/8bee8e7b-e21e-4332-be71-58f161a74b6b/en-13364-2001 (accessed on 12 August 2022).
46. *ASTM D 5731*; Standard Test Method for Determination of the Point Load Strength Index of Rock and Application to Rock Strength Classifications. American Society for Testing and Materials: West Conshohocken, PA, USA, 2008.
47. EN 14579 Natural Stone Test Methods—Determination of Sound Speed Propagation—European Standards. Available online: https://www.en-standard.eu/une-en-14579-2005-natural-stone-test-methods-determination-of-sound-speed-propagation/ (accessed on 10 August 2022).
48. EN 14146—Natural Stone Test Methods—Determination of the Dynamic Modulus of Elasticity (by Measuring the Fundamental Resonance Frequency). Available online: https://standards.globalspec.com/std/800632/EN14146 (accessed on 7 August 2022).
49. Bansa, H. Accelerated Ageing of Paper: Some Ideas on Its Practical Benefit. *Restaurator* **2002**, *23*, 106–117. [CrossRef]
50. Crewdson, M. Outdoor Weathering Must Verify Accelerated Testing. In Proceedings of the Annual Technical Conference—ANTEC, Newtown, CT, USA, 1–5 May 2011.
51. Vergari, S. *AM, Aeronautica Militare Italiana, La Radiazione Solare Globale e La Durata Del Soleggiamento in Italia Dal 1991 Al 2010*; ENEA: Rome, Italy, 2018.
52. EOTA TR 010, Exposure Procedure for Artificial Weathering, Technical Report. Available online: https://www.eota.eu/sites/default/files/uploads/Technical%20reports/tr010.pdf (accessed on 10 February 2023).
53. *ASTM D3424-11*; Standard Practice for Evaluating the Relative Lightfastness and Weatherability of Printed Matter. ASTM International: West Conshohocken, PA, USA, 2001.
54. Fookes, P.G.; Dearman, W.R.; Franklin, J.A. Some Engineering Aspects of Rock Weathering with Field Examples from Dartmoor and Elsewhere. *Q. J. Eng. Geol.* **1971**, *4*, 139–185. [CrossRef]
55. Alves, C.; Figueiredo, C.A.M.; Sanjurjo-Sánchez, J.; Hernández, A.C. Effects of Water on Natural Stone in the Built Environment—A Review. *Geosciences* **2021**, *11*, 459. [CrossRef]
56. Fahey, B.D. Frost Action and Hydration as Rock Weathering Mechanisms on Schist: A Laboratory Study. *Earth Surf. Process. Landf.* **1983**, *8*, 535–545. [CrossRef]
57. Kahraman, S.; Ulker, U.; Delibalta, M.S. A Quality Classification of Building Stones from P-Wave Velocity and Its Application to Stone Cutting with Gang Saws. *J. S. Afr. Inst. Min. Metall.* **2007**, *107*, 427–430. [CrossRef]
58. Amaral, P.M.; Fernandes, J.C.; Rosa, L.G. Weibull Statistical Analysis of Granite Bending Strength. *Rock Mech. Rock Eng.* **2008**, *41*, 917–928. [CrossRef]

59. Amaral, P.M.; Guerra Rosa, L.; Cruz Fernandes, J. Assessment of Fracture Toughness in Ornamental Stones. *Int. J. Rock Mech. Min. Sci.* **2008**, *45*, 554–563. [CrossRef]
60. Lo Monaco, A.; Marabelli, M.; Pelosi, C.; Picchio, R. Colour Measurements of Surfaces to Evaluate the Restoration Materials. In Proceedings of the O3A: Optics for Arts, Architecture, and Archaeology III, Munich, Germany, 25–26 May 2011.
61. Lisci, C.; Sitzia, F.; Pires, V.; Mirão, J. Building Stones Durability by UVA Radiation, Moisture and Spray Accelerated Weathering. *J. Build. Pathol. Rehabil.* **2022**, *7*, 60. [CrossRef]